Transient Voltage and Electric Field Distributions in Air Core Reactors

S. L. Varricchio
CEPEL - Electrical Energy Research Center
Caixa Postal 68007, Rio de Janeiro, RJ
21.944-970 - Brazil

N. H. C. Santiago
UFRJ - Federal University of Rio de Janeiro
Caixa Postal 68504, Rio de Janeiro, RJ
21.945-970 - Brazil

Abstract - **This work presents a computational model for the evaluation of transient voltage and longitudinal electric field distributions in single layer air core reactors. The influence of a grounded shielding concentric to the reactor is considered. The validity of the model is verified by comparing computed and measured voltage responses at three taps of a test reactor. Analyses showing the influence of the grounded shielding, front time and front wave shape of the applied voltage on the maximum longitudinal electric stresses along the reactor winding are presented.**

1. INTRODUCTION

The evaluation of transient voltage and longitudinal electric field distributions in equipment windings are important for their optimum electric insulation design.

The aim of this work is to develop an accurate model representing a simple single layer air core reactor. The knowledge acquired with the development and use of this model is an important basis for the development of accurate models of more complex equipment, such as three phases power transformers. In order to demonstrate that, a grounded shielding concentric to the reactor was modeled.

The accuracy of the model supports the authors' belief that this work is a relevant contribution to the general effort in modeling winding equipment.

2. EQUIVALENT ELECTRIC CIRCUIT

The lumped parameter model for the calculation of the voltage and electric field distributions is obtained by dividing the reactor into a number N of sections which are electrically and magnetically coupled [1,2,3]. This procedure leads to the equivalent circuit shown in Fig. 1.

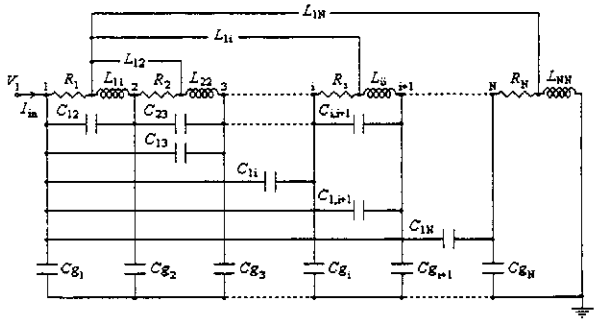

Fig. 1: Equivalent electric circuit

Lii : Self inductance of section i
Lij : Mutual inductance between sections i and j
Cgi : Capacitance to ground of section i
Cij : Mutual capacitance between sections i and j
Ri : Resistance of section i
V1 : Applied voltage
Iin : Input current

The influence of a grounded shielding cylinder, concentric to the reactor, is taken into account using the same procedure as for the reactor, i.e., dividing the shielding into a number M of sections that are electrically and magnetically coupled among themselves and the reactor sections.

3. COMPUTATION OF THE ELEMENTS OF THE EQUIVALENT CIRCUIT

3.1 Capacitance Matrix

The calculation of the capacitance matrix is done by using the Galerkin's method as describe in [3] or by an integral-equation technique described in [4].

The reactor and the grounded shielding are modeled by equipotential cylindrical surfaces divided into N and M cells (sections), respectively, which are not necessarily equal in length. The potential ϕ_i at a cell i is given by:

$$\phi_i = \sum_{j=1}^{N+M} p_{ij}\, Q_j\ ,\quad i = 1,\, N+M \qquad (1)$$

where Q_j is the total surface charge on cell j and p_{ij} is the potential coefficient between cells i and j.

Equation (1) forms a system of symmetric linear equations which can be written in a matrix form as:

$$[\phi] = [p][Q] \qquad (2)$$

Solving this system for the charges $[Q]$ yields:

$$[Q] = [c][\phi] \qquad (3)$$

where $[c] = [p]^{-1}$ is the partial capacitance coefficient matrix [4,5], since its elements represent the capacitance coefficient among parts (cells) of the equipotential cylindrical surfaces.

The capacitance matrix $[C]$ as well as the capacitances to ground of several cells are found from matrix $[c]$ [6].

The potential coefficient between two coaxial cylindrical cells [3], as shown in Fig. 2, is given by:

$$p_{ij} = \frac{1}{2\pi^2 \varepsilon_0\, l_i\, l_j} \int_{h_j - l_j}^{h_j + l_j} \int_{h_i - l_i}^{h_i + l_i} \left[\frac{F(k_1)}{A_1} - \frac{F(k_2)}{A_2} \right] dZ_i\, dZ_j \qquad (4)$$

where ε_0 is the air permittivity, $F(k_1)$ and $F(k_2)$ are complete elliptic integrals of the first kind with

$$A_1 = \left[\left(Z_i - Z_j\right)^2 + \left(R_i + R_j\right)^2 \right]^{1/2},\quad k_1 = \frac{2\left(R_i R_j\right)^{1/2}}{A_1}$$

$$A_2 = \left[\left(Z_i + Z_j\right)^2 + \left(R_i + R_j\right)^2 \right]^{1/2},\quad k_2 = \frac{2\left(R_i R_j\right)^{1/2}}{A_2}$$

In the expression (4) the ground plane is accounted for by the introduction of the image charges.

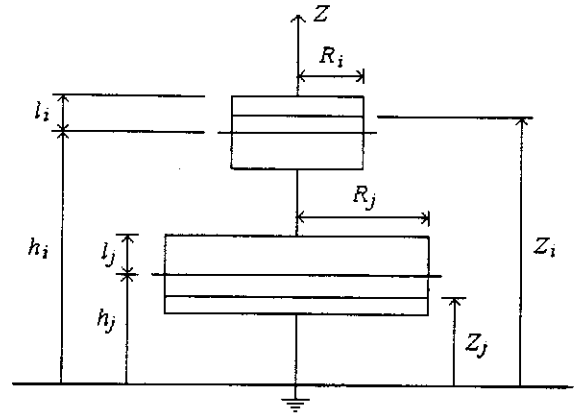

Fig. 2: Two coaxial cylindrical cells

3.2 Inductance Matrix

Consider the cells shown in Fig. 2 as two infinitesimally thin circular coaxial coils. From the application of Neumann's formula [6,7] to the turns localized at Z_i and Z_j, the mutual inductance between the coils is given by:

$$L_{ij} = \mu_0 n_i n_j \int_{h_j - l_j}^{h_j + l_j} \int_{h_i - l_i}^{h_i + l_i} \int_0^{\pi} \frac{R_i R_j \cos\varphi\, d\varphi\, dZ_i\, dZ_j}{\sqrt{R_i^2 + R_j^2 + \left(Z_i - Z_j\right)^2 - 2R_i R_j \cos\varphi}} \qquad (5)$$

where n_i and n_j are the number of turns per unit length and φ is the azimuthal angle. All of the other variables have the same meaning illustrated in Fig. 2.

The computation of the numerical value of L_{ij} is carried out by using a technique based on Bartky's transformation which is described in detail in [7].

3.3 Resistance Matrix

Since the model presents low sensitivity to the resistance frequency dependence [1,3], the d.c. values of R_i are used.

4. SOLUTION OF THE EQUIVALENT CIRCUIT

The numerical technique used in solving the electric equivalent circuit shown in Fig. 1 is based on two variable sets. The first set is formed by the total input current and by the voltages at the numbered nodes from 2 to N. The second set is formed by the currents through the inductive branches of the circuit.

Thus, two matricial equations involving these variable sets are necessary. The first equation is obtained by establishing the relationship between the two variable sets by means of the resistive and inductive elements and the second equation by means of the capacitive elements.

The discretization of the circuit equations is achieved by applying the trapezoidal integration rule.

For the consideration of a grounded shielding concentric to the reactor, it is necessary to include another variable set. This new set is formed by the circulating induced currents at the M sections of the grounded shielding, according to the discretization shown in Fig. 3. These currents are induced by the magnetic coupling between the reactor winding and the grounded shielding.

Further details of the mathematical development are given in [2,3].

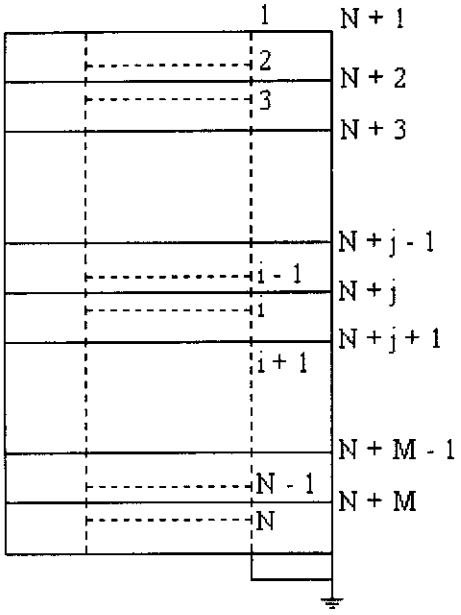

Fig. 3: Discretization of the system formed by the reactor and the grounded shielding

5. EXPERIMENTAL VERIFICATION OF THE THEORETICAL MODEL

In the following a brief description of the experimental setup is given. In order to show the validity of the model, a small sample of the comparative cases between the experimental and computed results is presented. Additional details are given in [1,2,3].

5.1 Experimental Setup

A test reactor and two shieldings were built. The dimensions of the reactor are shown in Table I.

Table I: Reactor dimensions

Length (m)		1.0
Diameter (m)		0.110
Wire Diameter (mm)		0.813
Number of turns		1130
Height above ground (m)		0.150
Measuring tap positions from reactor top (m)	Tap 1	0.2
	Tap 2	0.5
	Tap 3	0.8

The shieldings consisted of thin aluminum cylinders with equal lengths of 1.0 m and diameters of 0.26 m and 0.22 m.

Three reactor configurations were used, as follows:

Conf. 1 - Reactor without grounded shielding.
Conf. 2 - Reactor with a grounded shielding of 0.26 m diam.
Conf. 3 - Reactor with a grounded shielding of 0.22 m diam.

The applied voltage wave shapes were produced by two low voltage sources (impulse and step wave shape generators).

Measurements were performed using a digital oscilloscope with two probes. One probe was used to measure the applied voltage wave shape (V_1) and the other one was used to measure the voltage response in one of the measuring taps as shown in Fig. 4.

(a)

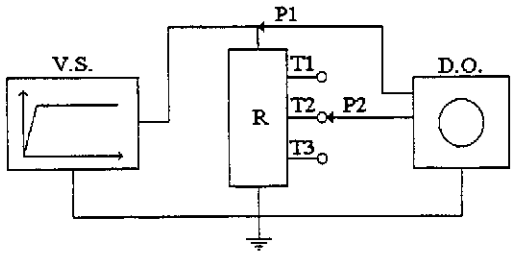

V.S. : Voltage source
D.O. : Digital oscilloscope
R : Reactor with/without grounded shielding
P1, P2 : Probes
T1, T2, T3 : Measuring taps

(b)

Fig. 4: Experimental setup: (a) photo, (b) schematic diagram

5.2 Comparison between Measured and Computed Voltage Responses

Fig. 5 shows the measured and computed voltage responses at taps 1 and 3 for an impulse voltage applied to the test reactor as in Conf. 2. The front time and time to half value [8] for the impulse voltage were 0.750 μs and 44 μs, respectively.

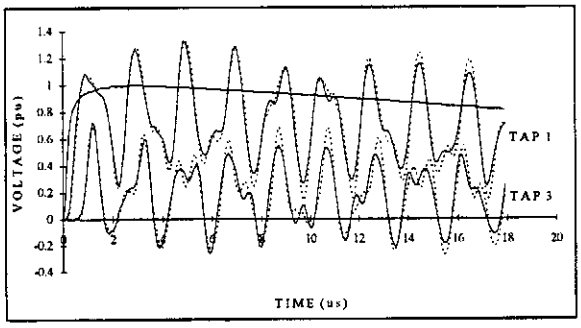

Fig. 5: Measured (full line) and computed (dotted line) voltages responses

6. EVALUATION OF THE LONGITUDINAL ELECTRIC FIELD ON THE REACTOR WINDING

The relationship among the electric and magnetic potentials and the electric field is given by:

$$\vec{E} = -\nabla V - \frac{\partial \vec{A}}{\partial t} \tag{6}$$

Where $\vec{E}$ is the electric field, V is the electric scalar potential, $\vec{A}$ is the magnetic vector potential and t is the time.

For cylindrical windings which present current distributions characterized by $J_z = 0$, similarly to the winding of the test reactor, the following applies:

$$A_z = 0 \tag{7}$$

where J_z is the longitudinal component of the superficial current density, $\vec{J}$, and A_z is the longitudinal component of $\vec{A}$.

Regarding Fig. 6 and equations (6) and (7), one has the following expression for the longitudinal component of the electric field E_z on the reactor winding:

$$E_z(r_0, z, t) = -\frac{\partial V(r_0, z, t)}{\partial z} \tag{8}$$

Considering a specific time instant, the above equation can be approximated by:

$$E_z(z_i) = \frac{V(i+1) - V(i-1)}{2\Delta z} \tag{9}$$

where:

z_i → Position on the reactor winding corresponding to node i of the equivalent electric circuit.

$E_z(z_i)$ → Longitudinal component of the electric field at position z_i on the reactor winding.

$V(i)$ → Voltage at node i of the equivalent electric circuit corresponding to position z_i on the reactor winding.

Δz → Distance between positions corresponding to two consecutive nodes of the equivalent electric circuit.

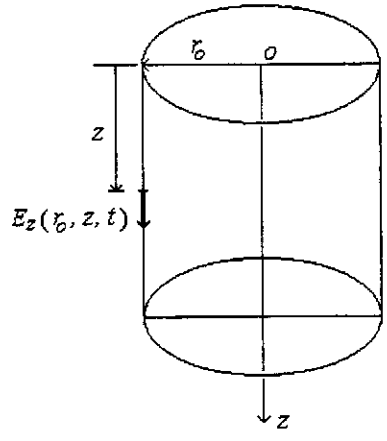

Fig. 6: Electric field on the reactor winding

Figs. 7(a) and (b) show spatial distributions of voltage and electric field, respectively, along the winding for a 0.750/44 μs impulse voltage applied to the test reactor as in Conf. 2. These distributions were computed at time instants which represent, approximately, 30%, 60% and 90% of the front time of the applied voltage.

In Fig. 7(b), E_{unif} represents the electric field due to a uniform voltage distribution, given by:

$$E_{unif} = \frac{V_{max}}{l} \qquad (10)$$

Where V_{max} is the peak value of the applied voltage and l is the total test reactor length.

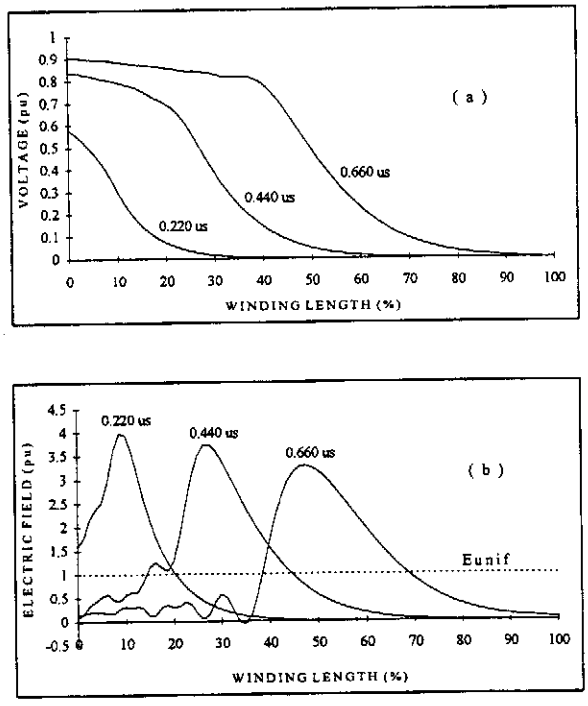

Fig. 7: Spatial distributions of (a) voltage and (b) electric field

7. INFLUENCE OF SOME FACTORS ON THE MAXIMUM LONGITUDINAL ELECTRIC STRESSES ALONG THE WINDING

7.1 Grounded Shielding

Fig. 8 shows the envelopes of the longitudinal electric field along the winding for an impulse voltage applied to the test reactor for all configurations. These envelopes represent the maximum values of the longitudinal electric field which occurred along the winding during the application of the applied voltage.

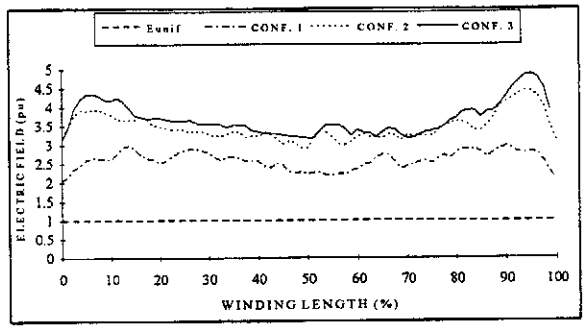

Fig. 8: Influence of the grounded shielding on the maximum longitudinal electric stresses

7.2 Front Time

Fig. 9 shows the envelopes of the longitudinal electric field along the winding of the test reactor as in Conf. 2. These envelopes were due to 0.750/44 μs, 0.950/44 μs and 1.150/44 μs applied voltages. The same behavior was found for the remaining configurations.

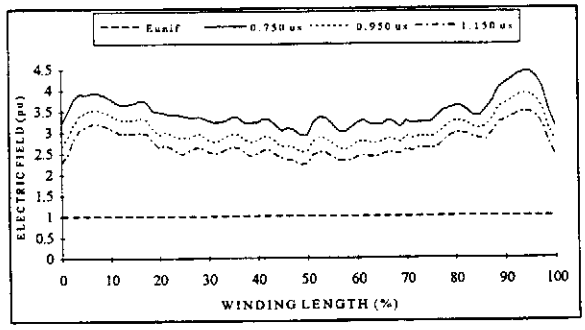

Fig. 9: Influence of the front time on the maximum longitudinal electric stresses

7.3 Front Wave Shape

Fig. 10 shows two applied voltage wave shapes which have the same front time and time to half value, i.e., 0.750/44 μs.

Fig. 11 shows the envelopes of the longitudinal electric field along the winding for the test reactor as in Conf. 2. These envelopes were due to the applied voltage wave shapes shown in Fig. 10.

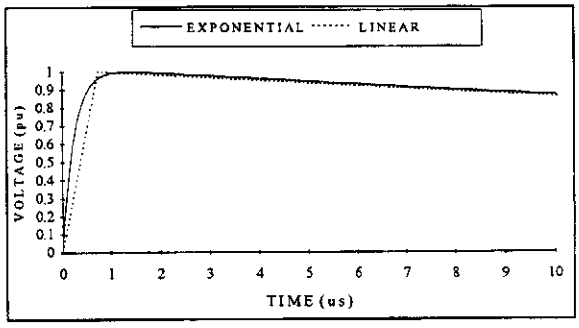

Fig. 10: 0.750/44 μs impulse voltages with different front wave shapes

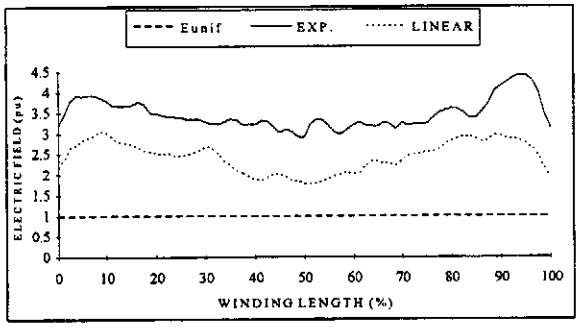

Fig. 11: Influence of the front wave shape on the maximum longitudinal electric stresses

8. CONCLUSIONS

An efficient discrete model to compute transient voltage and longitudinal electric field distributions in single air core reactor has been developed.

The validity and accuracy of the model were verified by comparing experimental and computational results.

A grounded shielding concentric to the reactor increases the maximum longitudinal electric stresses along the winding (Fig. 8). It must be pointed out that the stresses are higher for Configuration 3, showing that the higher the values of the winding capacitances to ground, the higher the maximum longitudinal electric stresses along the winding.

Regarding Figs. 9 and 11, one can conclude that the maximum longitudinal electric stresses along the winding are strongly dependent on the front time and the front wave shape of the applied voltage.

9. REFERENCES

[1] S. L. Varricchio, N. H. C. Santiago, "Transient Voltage Distribution in Air Core Reactors", Eighth International Symposium on High Voltage Engineering, No. 68.06, pp. 221-224, Yokohama, Japan, August 23-27, 1993.

[2] S. L. Varricchio, N. H. C. Santiago, "Electrical Strength in Air Core Reactors", Proceedings of the 4th International Conference on Properties and Applications of Dielectric Materials, No. 7236, pp. 876-879, Brisbane, Australia, July 3-8, 1994.

[3] S. L. Varricchio, "Transient Voltage Distribution in Air Core Reactors", M.Sc. Thesis - Federal University of Rio de Janeiro, Rio de Janeiro, Brazil, April, 1994 (in Portuguese).

[4] Albert E. Ruehli and Pierce A. Brennan, "Efficient Capacitance Calculation for Three-Dimensional Multiconductor Systems", IEEE Trans. Microwave Theory Tech., Vol. MTT-21, No. 2, pp. 76-82, 1973.

[5] A. E. Ruehli, "Electrical Analysis of Interconnections in a Solid-State Circuit Environment", IEEE Int. Solid-State Circuit Conf. Dig., pp. 64-65, 1972.

[6] S. Ramo, J. R. Whinnery and T. V. Duzer, Fields and Waves in Communication Electronics. New York: Wiley, 1965.

[7] Tharwat H. Fawzi and P. E. Burke, "The Accurate Computation of Self and Mutual Inductances of Circular Coils", IEEE Trans., Vol. PAS-97, No. 2, pp. 464-468, 1978.

[8] IEC 60-1, "High-voltage test techniques - Part 1: General definitions and test requirements", 1989.